SO_2 as a possible proxy for volcanic ash in aviation hazard avoidance

T. M. Sears,[1] G. E. Thomas,[1] E. Carboni,[1] A. J. A. Smith,[1] and R. G. Grainger[1]

Received 6 September 2012; revised 26 April 2013; accepted 16 May 2013.

[1] Airborne volcanic ash poses a significant danger to aircraft, but is difficult to quantify accurately using satellite data, while sulphur dioxide is much easier to detect accurately, but is much less of a direct hazard to aviation. This paper investigates the reliability of using SO_2 as a proxy for the location of volcanic ash, using an SO_2 retrieval from the Infrared Atmospheric Sounding Interferometer (IASI) and ash detections from IASI and the Advanced Along Track Scanning Radiometer (AATSR). Using a numerical "missed ash fraction" applied to the eruptions of Eyjafjallajökull in 2010 and Puyehue-Cordón Caulle in 2011 reveals that the SO_2 flag typically misses ∼30% of the detectable ash. Furthermore, the missed ash fraction is found to be highly variable, both between the two eruptions and over the course of each eruption, with values of over 80% found on some days. The detection threshold of the AATSR ash flag is also investigated using radiative transfer calculations, allowing the threshold of the IASI flag to be inferred, and these are related to the ash contamination levels.

Citation: Sears, T. M., G. E. Thomas, E. Carboni, A. J. A. Smith, and R. G. Grainger (2013), SO_2 as a possible proxy for volcanic ash in aviation hazard avoidance, *J. Geophys. Res. Atmos.*, *118*, doi:10.1002/jgrd.50505.

1. Introduction

1.1. Motivation

[2] Volcanic eruptions can release large quantities (Tg) of volcanic ash and also gases such as water vapor, carbon dioxide, and sulphur dioxide into the atmosphere [*Robock*, 2000]. These eruptions can occur in remote locations which are not the focus of regular measurements, and the first indications of such events often come from satellite observations. These satellite measurements are key tools in detecting and tracking both ash and gases from eruptions. Sulphur dioxide (SO_2) is often used as an indication of volcanic hazard when using satellite observations [e.g., *Carn et al*., 2009], under the assumption that ash and SO_2 are collocated passive tracers. However, it has been shown that this assumption does not hold in general. This is usually due to the differing densities of ash and SO_2 coupled with vertical wind shear causing lateral separation of the ash and gas plumes [e.g., *Schneider et al*.,1999; *Prata and Kerkmann*, 2007; *Rose et al*., 2000; *Thomas and Prata*, 2011]. While previous work has demonstrated that separation does occur, in this work we introduce a numerical missed ash fraction, defined in section 2, which allows a quantitative assessment of the effectiveness of SO_2 as a proxy for ash and its evolution throughout an eruption period. We use the eruptions of Eyjafjallajökull in 2010 and Puyehue in 2011 as case studies, using ash flags derived from the Advanced Along Track Scanning Radiometer (AATSR), the Infrared Atmospheric Sounding Interferometer (IASI) satellite instruments, and an SO_2 flag derived from IASI.

[3] The volcanic ash hazard to aircraft arises from a range of physical damage done by the ash. The most significant of these is that, if ash enters a jet engine, it melts due to the high operating temperatures (the melting point of volcanic ash is ∼ 1100 K while typical operating temperatures of aircraft engines are ∼ 1400 K, [*Vogel et al.*, 2011]), and then adheres to moving parts of the turbine, causing them to jam and, potentially, the engine to stall. One of the most famous examples of this, and the one which first brought the danger of ash to the media's attention, was the case in June 1982 of a British Airways Boeing 747-200 that lost power to all four engines mid-flight. It glided for 16 min before the crew managed to restart three of the four engines and make an emergency landing at Jakarta, Indonesia. Following the incident, investigation of the engines revealed significant damage due to volcanic ash from the nearby Mt. Galunggung, which was erupting at the time [*ICAO*, 2007]. Another similar incident occurred 3 weeks later, and another during the 1989 eruption of Mt. Redoubt, Alaska. These further encounters confirmed that the 1982 British Airways incident was not a one-off event, and that any volcanic ash encounter is likely to have serious consequences [*Casadevall*, 1994]. Other effects caused by ash encounters include the sandblasting of the windscreen and landing lights, affecting visibility, the blocking of pitot tubes causing flight instruments to show incorrect readings, and interference with the communication systems in the aircraft due to the charged nature of the ash particles [*Casadevall and Murray*, 2000]. Between the years 1970 and 2000, over 90 aircraft sustained damage as a direct result of flying through

[1]Atmospheric, Oceanic and Planetary Physics, University of Oxford, Oxford, UK.

Corresponding author: G. E. Thomas, Atmospheric, Oceanic and Planetary Physics, University of Oxford, Oxford, OX1 3PU, UK. (gthomas@atm.ox.ac.uk)

2169-897X/13/10.1002/jgrd.50505

clouds of volcanic ash. The danger of the ash is compounded by the fact that it is invisible on aircraft radar and so, particularly at night, there is no way of pilots knowing if they are heading for a hazardous cloud until they reach it and symptoms begin.

[4] In addition to the potential loss of life and assets, the financial implications of any accident would be severe, as is the cost associated with any prolonged closure of airspace or airports as a result of a volcanic eruption—being able to accurately predict ash cloud movements could therefore bring financial benefits to airlines. According to the International Air Transport Association, during the 2010 eruption of Eyjafjallajökull in Iceland, the closure of airspace over much of Europe caused a loss to the airline industry of an estimated US$1.7 billion (The International Air Transport Association press release no. 15, 21 April 2010: http://www.iata.org/pressroom/pr/Pages/2010-04-21-01.aspx).

[5] Although the immediate negative effects are not as serious as those from ash, SO_2, which is also emitted in large amounts from volcanoes, can also have a detrimental effect on aircraft, leading to degradation of parts and hence costly repairs [*Vogel et al.*, 2011]. During 1983–1984, Japan Airlines saw an increase from 1 to 30–40 in replacement cockpit windows due to crazing. This was attributed to acidic conditions in the stratosphere due to long-lived stratospheric sulphuric acid (H_2SO_4) aerosols from the 1982 eruption of the El Chichón Volcano, Mexico [*Bernard and Rose*, 1990].

[6] As well as inconveniences to air travel, SO_2 has a negative effect on the environment, mainly through the following reactions:

$$SO_2 + OH + M \rightarrow HSO_3 + M, \quad (1)$$

$$HSO_3 + O_2 \rightarrow HO_2 + SO_3, \quad (2)$$

$$SO_3 + H_2O + M \rightarrow H_2SO_4 + M, \quad (3)$$

where M denotes either N_2 or O_2. The lifetime of SO_2 depends strongly on the availability of oxidizing agents, in particular the presence of water vapor, but is typically a few days in the troposphere. The net result is the production of sulphuric acid, which forms sulphate aerosol and, in high concentrations, acid rain [*Ward*, 2009].

[7] While ash is the primary concern for air travel, SO_2 is, in general, easier to identify and quantify using remote sensing, since there is good sensitivity to absorption by SO_2 in both the ultraviolet and infrared regions, meaning there are many different satellite instruments which can be used to detect it. Also, background levels are generally low (less than 1 DU, compared to volcanic column amounts >1 DU within volcanic plumes over hundreds or thousands of kilometers downwind of an explosive eruption) and as a result, the majority of positive detections will be from volcanic activity [*Carn et al.*, 2009; *Zehner*, 2012]. Ash detection can be hampered by the presence of overlying ice or water clouds causing the ash to be obscured and, in addition to this, high concentrations of water vapor in clouds can sometimes be flagged as ash, thus causing false positive ash detections. Also, the presence of ice within the ash cloud can affect identification [*Clarisse et al.*, 2010]. Another difficulty with the detection of ash is that sometimes ash clouds do not display sufficient thermal contrast to distinguish them from the underlying terrain and so do not show up in satellite images [*Pergola et al.*, 2004].

[8] At the time of the 2010 eruption of Eyjafjallajökull, the London Volcanic Ash Advisory Centre (LVAAC), which was responsible for determining the areas likely to be affected by ash, did not use quantitative data from satellites for this purpose due to the difficulties in reliably quantifying ash. Instead, it relied upon a sophisticated Lagrangian particle dispersion model in order to predict the trajectories of the ash particles, with satellite images simply being used to verify the results obtained from the dispersion model [*Webster et al.*, 2012]. The significant uncertainties in the model meant that a conservative estimate of the location and concentration of ash had to be taken in order to eliminate the possibility of any aircraft encountering unforecast ash. More quantitative estimates from satellite data are being developed to work alongside the dispersion model to improve ash forecasts [*Francis et al.*, 2012], but the difficulty of determining ash properties from satellite data remains. The use of satellite SO_2 products by the VAACs is already well developed, with the Support to Aviation Control Service (SACS) regularly supplying near-real-time SO_2 products from a range of UV and infrared satellite sensors [*van der A et al.*, 2010], so being able to reliably use SO_2 as a proxy for ash would be advantageous to VAACs. Although there have been several studies comparing ash and SO_2 emissions from various volcanic eruptions [*Schneider et al.*, 1999; *Prata and Kerkmann*, 2007; *Rose et al.*, 2000; *Thomas and Prata*, 2011], but these have been largely qualitative. In this work we attempt to provide a quantitative measure of the effectiveness of satellite SO_2 products as an ash proxy.

1.2. Retrieval Techniques

[9] The satellite used for the majority of the SO_2 and ash detection for the eruptions studied for the purposes of this paper was the Infrared Atmospheric Sounding Interferometer (IASI) on board the EUMETSAT Metop-A satellite. However, for comparison, an ash retrieval was also used from the Advanced Along Track Scanning Radiometer (AATSR), which was stationed on board the now-defunct ENVISAT satellite from 2002 until communication was lost with the satellite in April 2012.

1.2.1. IASI

[10] IASI completes a global scan once every 12 h. The instrument works in the thermal infrared region and uses a Fourier transform spectrometer covering the spectral range 645–2760 cm^{-1} (3.62–15.5 μm). Its field-of-view consists of four circular pixels, each of diameter 12 km at the surface, within a square of 50 km × 50 km, step-scanned across track in 30 steps, giving a swath of approximately 2000 km. *Clerbaux et al.* [2009] present a diagram of the setup in their Figure 1. IASI has been widely used for the detection of SO_2, and a brightness temperature index based on channels around the so-called ν_3 band centered at 7.3 μm [*Clarisse et al.*, 2008] is now included in the SACS system.

[11] Both the SO_2 and ash detection schemes used with IASI in this work rely on the approach described by *Walker et al.* [2011, 2012]. The scheme makes use of a generalized error covariance that contains not only the instrument noise, but covariance due to interfering trace gases and broadband scatterers (such as aerosols and clouds) that should be unrelated to the required retrieved property. Since these signals are included in the covariance, they need not be retrieved nor

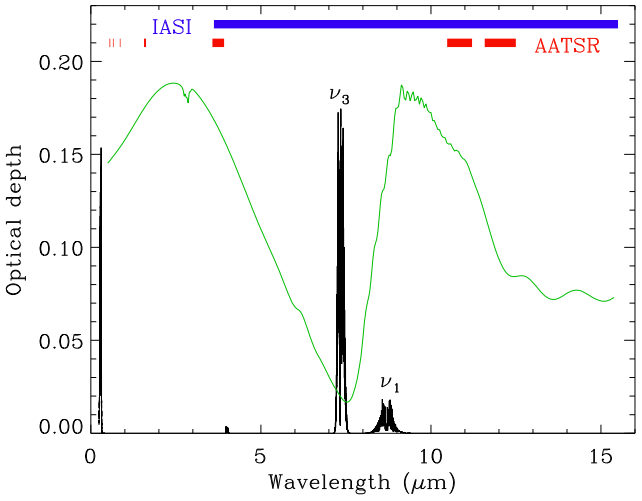

Figure 1. Optical depths at different wavelengths for SO_2 (assuming 5 DU centered at an altitude of 15 km, shown in black) and ash (assuming a plume thickness of 1 km, an ash particle effective radius of 2.26 μm and a particle number density of 10 cm^{-3}, shown in green). Also shown are the regions sampled by both IASI (in blue) and AATSR (in red). SO_2 short wave data are taken from *Bogumil et al.* [2003].

their variance taken account of in the forward model of the atmosphere.

[12] Using the notation of *Rodgers* [2000], we define the measured spectra, **y**, as a function of the forward model, $F(x, \mathbf{b})$:

$$\mathbf{y} = F(x, \mathbf{b}) + \epsilon_{\text{random}} + \epsilon_{\text{systematic}}, \quad (4)$$

where x is the quantity of interest (either optical depth of volcanic ash or column amount of SO_2), **b** contains the properties of some background atmospheric state, and ϵ indicates a vector of errors in $F(x, \mathbf{b})$. The value of x is calculated by linearizing about some fixed value, x_0, leading to the following expression:

$$\mathbf{y} - F(x_0, \mathbf{b}) = \mathbf{K}(x - x_0) + \epsilon_{\text{random}} + \epsilon_{\text{systematic}}, \quad (5)$$

where **K** is the Jacobian of **y** with respect to x. The least squares estimate of x can be obtained by

$$x = x_0 + \left(\mathbf{K}^T \mathbf{S}_\epsilon^{-1} \mathbf{K}\right)^{-1} \mathbf{K}^T \mathbf{S}_\epsilon^{-1} \left(\mathbf{y} - F(x_0, \mathbf{b})\right). \quad (6)$$

The error covariance matrix, $\mathbf{S}_\epsilon$, is built up from IASI measurements in the same geographical area and time of year when no volcanic signals are present.

[13] This approach has the advantage of making use of the high spectral resolution provided by the IASI instrument, while not sacrificing computational speed. The retrieved value of x does, however, rely heavily on the choice of linearization point and so requires independent calibration measurements of x to provide accurate numerical results.

[14] The ν_3 absorption features (at 7.3 μm) are used in the SO_2 detection scheme [*Walker et al.*, 2012]. This detection scheme is complemented with an SO_2 column amount optimal estimation retrieval, which uses both the 8.7 μm ν_1 and ν_2 bands [*Carboni et al.*, 2012]. The latter has the strongest absorption; however, it lies within a strong absorption band for water vapor and as a result is not very sensitive to emission from the lower atmosphere. The 8.7 μm band is weaker, but lies in an atmospheric window and so contains a total column SO_2 signal. By using both bands, the retrieval has some sensitivity to plume height, as well as a column amount.

[15] *Walker et al.* [2012] performed a sensitivity study of this IASI SO_2 detection using data from the 2010 Eyjafjallajökull eruption. They found that the detection threshold decreased exponentially with height; plumes that lay below 2 km provided a threshold of 17 DU, but this rapidly improved to 3.3 DU between 2–4 km, 1.3 DU for 4–6 km and reached 0.3 DU for the tropopause cold point. This sensitivity is approximately an order of magnitude better than earlier IASI SO_2 flags [*Clerbaux et al.*, 2009; *Zehner*, 2012] and was able to reliably detect the plume from the earliest explosive stages of the eruption.

[16] The application of this method to volcanic ash detection with IASI is a more recent development, and the approach taken is similar to that described by *Clarisse et al.* [2012]. In this case the x defined in equation 4 is the volcanic ash optical depth, τ, and a broad region of the IASI spectrum from 7.8–14.7 μm is used. The value of τ retrieved strongly depends on the linearization point, τ_0 chosen, which limits its usefulness in determining the amount of ash present. However, the method has been found to be a useful ash flag for the presence of ash clouds, as elevated ash amounts are clearly visible above the noise in the retrieved fields.

1.2.2. AATSR

[17] AATSR measures radiance in seven different channels ranging from the visible to the thermal infrared. One of the defining features of AATSR is the fact that it takes two images, one of which is a nadir view and the other a forward view at a zenith angle of 55°. This allows the radiance from the surface and the radiance from particles in the atmosphere to be distinguished from each other, since in each view the signal has a different atmospheric path length. Following any particular forward view image, it takes ∼ 150 s for the satellite to be in a position such that the nadir view samples the same region, and as such the two views are near-simultaneous. The instrument has a swath width of 512 km (with 555 pixels across the nadir swath and 371 pixels across the forward swath), and global coverage is achieved every 3–6 days. The spatial resolution of this instrument is better than that of IASI (∼ 1 km as opposed to ∼ 12 km), but the small swath width and relatively infrequent coverage of any particular area reduces the number of coincident measurements from AATSR, hence the desire for an IASI ash retrieval. A full description of the AATSR instrument is given by *Llewellyn Jones* [1993] and *Smith et al.* [2001].

[18] The measured radiances were converted into ash heights using the parallax between the two images. The brightness temperature difference between the 10.8 μm and the 12 μm channels can be used as a rough, qualitative indication of the amount of ash present in each pixel. This brightness temperature difference gives a negative value where ash is present, but a positive value where water vapor or ice (i.e., cloud) is present, as described by *Prata* [1989] and *Wen and Rose* [1994]. In this work, a pixel was flagged as ash if both of the following conditions were met:

$$BT_{10.8} - BT_{12.0} < -0.1K \quad (7)$$

$$BT_{10.8} - BT_{3.7} < -20.0K. \quad (8)$$

The additional condition on the brightness temperature difference between the 3.7 μm and 10.8 μm channels is imposed as a means of removing false detections, as high, cold ice cloud can also produce a negative 10.8–12 μm brightness temperature difference.

1.2.3. Comparison of Instruments

[19] Figure 1 shows the spectral optical depth for a 5 DU column of SO_2, with a Gaussian altitude distribution centered around 15 km, and a 1 km thick ash plume. The horizontal bars at the top of the plot show the wavelengths covered by IASI and AATSR. From this it can clearly be seen that SO_2 has a spectral-line based signature, while the corresponding result for ash is a broadband spectrum. Furthermore, all seven of the AATSR channels are completely clear from the SO_2 spectral features, meaning that the AATSR ash retrieval is unlikely to be affected by any SO_2 present. The spectral region sampled by IASI, however, encompasses both ash and SO_2 features, which suggests that the presence of ash may affect the IASI SO_2 retrieval, and vice versa. This is found to be the case where ash concentrations are particularly high, such as very close to volcanoes themselves, and a method to reduce this problem is discussed later in relation to the 2011 eruption of Puyehue.

2. Methodology

2.1. Determining Collocation

[20] In order to quantify the collocation of ash and SO_2, we define a "missed ash fraction" (as well as an analogous missed SO_2 fraction), which can be used to compare any pair of satellite derived ash and SO_2 products. We define the missed ash fraction as the ratio of the area containing ash, but no detectable SO_2 to the total area containing ash. Under the assumption that the ash-flag detection thresholds are not changed by the presence of SO_2, the following procedure can be used to estimate the missed ash fraction.

[21] The products are first regridded onto a common spatial grid, where each grid cell is flagged as containing ash and/or SO_2 if it contains any satellite pixels with a positive detection from each flag. The two products can then be directly compared on a point by point basis. Then, having limited the set of grid cells to those present in both ash and SO_2 products, the missed ash fraction is then defined as the ratio of the number of pixels which have been flagged as ash but not SO_2, over the total number of pixels flagged as ash (i.e., pixels flagged as both ash and SO_2 and those flagged solely as ash). This was carried out for two groups of orbits per day (morning and afternoon) using the IASI data and could be verified by AATSR readings where available.

2.2. Ash Detection Thresholds

[22] One major issue which needed to be addressed was to determine how the lower ash detection threshold of the satellites corresponds to the lowest designated safe level of ash for aircraft flight. This is difficult to determine using the IASI ash flag, as it uses an empirical statistical approach not easily simulated with radiative transfer; however, it can be estimated for AATSR. Using this value and studying corresponding plots from the two satellites allows a relative threshold of IASI compared to AATSR to be determined.

[23] Although there is no official international "no fly limit," the International Civil Aviation Organization (ICAO) and the UK Civil Aviation Authority (CAA) have defined three categories of ash concentration, ρ: low contamination ($0.2 < \rho \leq 2\,\mathrm{mg\,m^{-3}}$), medium contamination ($2 < \rho < 4\,\mathrm{mg\,m^{-3}}$) and high contamination ($\rho \geq 4\,\mathrm{mg\,m^{-3}}$) [*Civil Aviation Authority*, 2011]. Areas of low contamination may be entered by aircraft and are generally considered safe, while those of medium and high contamination require a safety case to be completed by airlines before flying through them, and, in general, commercial airlines only have this safety case for the medium contamination ash situation. Thus the "no fly" limit is effectively $4\,\mathrm{mg\,m^{-3}}$. The thresholds are largely scientifically unverified due to the difficulty in determining them without putting lives at risk, and as a result a "zero tolerance" approach is often taken (and is advised by the ICAO, [*International Federation of Airline Pilots' Associations*, 2011]) in order to avoid any possible incidents. Initially, a zero tolerance blanket restriction was put in place during the 2010 eruption of Eyjafjallajökull, but following pressure from airlines, the CAA introduced the above limits on 18 May 2010. Using a Lagrangian transport model constrained by satellite observations of the ash cloud, *Stohl et al.* [2011] showed that, at a latitude-longitude resolution of 0.25 × 0.25° (approximately 450 km^2 at European latitudes), the limit of $4\,\mathrm{mg\,m^{-3}}$ was only very rarely exceeded, and even that of $2\,\mathrm{mg\,m^{-3}}$ was only exceeded on two occasions, and only over 1.5% and 0.9% of Europe, respectively. This result does not discount subgrid concentrations that were significantly above these limits, and the difference in spatial resolution between the resolution used by *Stohl et al.* [2011] and the 1 km^2 pixels size of AATSR should be noted.

[24] Evidence from engine tests suggests that the concentrations of ash which caused engine flameout in the 1989 encounter with ash from Mt. Redoubt were as high as $2\,\mathrm{g\,m^{-3}}$ [*Przedpelski and Casadevall*, 1994]. The Institution of Mechanical Engineers have calculated, based on the fact that 80 kg of ash were found deposited in each turbine engine, that if the plane had been flying in the same conditions but with only $4\,\mathrm{mg\,m^{-3}}$ (the currently accepted absolute no-fly limit) then only 160 g of ash would have made its way into the engines, suggesting a hugely cautious safety threshold [*Institution of Mechanical Engineers*, 2010]. For these reasons, many believe the thresholds given above are too severe. Nevertheless, until more definitive tests can be carried out on aircraft engines, and satellite measurements of ash concentrations made with only negligible uncertainty, then it will remain necessary to be over-cautious in this matter.

[25] By assuming the ash lies in a homogeneous layer of uniform thickness s then the optical depth τ of the plume can be estimated as

$$\tau = \int_0^s \beta \mathrm{d}z \approx \beta s$$

where β is the extinction coefficient. Using spectral extinction measurements of ash from Mt. Aso, Japan (D. M. Peters, personal communication, 2012), the value of β obtained for the ash is $0.03\,\mathrm{km^{-1}}$ at 550 nm assuming a concentration of 1 particle $\mathrm{cm^{-3}}$. Aso ash extinctions were used as a proxy for Eyjafjallajökull, as the measurements were readily available at the time—subsequent comparison of spectra

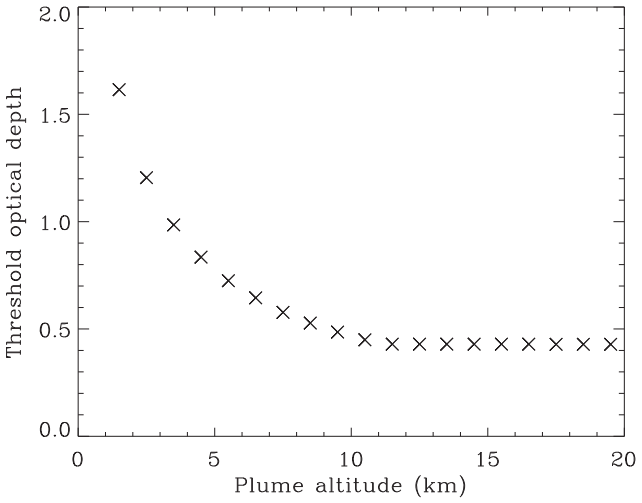

Figure 2. Variation of the threshold optical depth for ash detection (calculated using the DISORT model) with plume altitude, assuming a particle effective radius of 2.26 μm and a plume thickness of 1 km.

from Eyjafjallajökull ash samples have shown it to be similar enough for this analysis to be considered valid. This can then be used to calculate an expression for the number density of ash particles as a function of optical depth and plume thickness. A range of in situ and ground based estimates of the particle size distribution within the distal ash cloud from Eyjafjallajökull are available. Measurements from the Facility for Airborne Atmospheric Measurement (FAAM) BAe 146 aircraft and AERONET stations in North Western Europe [*Johnson et al.*, 2012; *Derimian et al.*, 2012] both suggest an ash effective radius of ∼1.3–1.6 μm, while measurements from the DLR Falcon aircraft found larger particles, with an effective radius of 6.3 μm [*Turnbull et al.*, 2012]. The effect radius assumed in calculating the radiative properties of the Aso ash was 2.26 μm.

[26] Using the Discrete Ordinates Radiative Transfer (DISORT) model [*Stamnes et al.*, 1988] with the assumed effective radius of 2.26 μm and plume thickness of 1 km, it was discovered that the threshold ash detection optical depth for AATSR varies as a function of ash altitude, as shown in Figure 2. If it is assumed that most of the ash lies at an altitude of between 3 and 6 km, as seems to be the case from the AATSR height retrievals [*Grainger et al.*, 2013], as well as in situ [*Turnbull et al.*, 2012] and lidar [*Marenco et al.*, 2011] aircraft measurements, then it can be seen that the threshold optical depth can be taken very approximately as equal to 1.

[27] Using an ash density value of $\rho_{ash} = 2400\,kg\,m^{-3}$ [*Niemeier et al.*, 2009] allows a relationship between optical depth, layer depth, and ash concentration to be found (Figure 3). The approximate detection threshold is marked as a white vertical line in the figure, and the black line indicates the ICAO/CAA threshold of $4\,mg\,m^{-3}$. Any points below this line denote ash concentrations above the high contamination threshold. It is stated in *Winker et al.* [2012] that the ash plume from Eyjafjallajökull was between 0.4 and 1 km thick at altitudes between 1 and 7 km. It can be seen that at a plume thickness of 0.4 km, there is a region to the left of the detection threshold, which is still within the no fly concentration region. Thus, there is potentially some areas of high contamination which are not being detected by AATSR. Although at a thickness of 1 km this is no longer the case, the fact that the relevant plume thickness range is right on the boundary between all significant ash being detected and some being missed means that, in reality, the chances are that some ash in the plume will be missed by AATSR. It can also be seen from Figure 3 that for all plumes with a thickness less than ∼ 700 m, all of the ash which is detected will occur in concentrations higher than the $4\,mg\,m^{-3}$ threshold, so no ash flags should be ignored unless there is very strong evidence that it is a false positive detection.

[28] This calculation has assumed throughout the presence of ash in isolation, and so it should be mentioned again that the presence of ice or water cloud can affect the results and hence can alter this detection threshold, as can the presence of an ice/ash mixture.

[29] By looking at the amounts of ash detected by the IASI and AATSR on the same day, an estimate of the relative ash detection thresholds can be made. As an example, Figure 4 shows these results for 9 May 2010 during the Eyjafjallajökull eruption, calculated using a grid box of side length equivalent to 0.5° longitude and latitude. The Metop and ENVISAT platforms are both in sun-synchronous orbits, with local equatorial crossing times of 9:30 and 10:00, respectively. Thus, although there will be some evolution of the scene during this interval, observations of the ash cloud between the two instruments should be highly correlated at this spatial scale. The red points in Figure 4 show where both satellites agree that ash is present. The green and blue points at the edges of the plume denote where just IASI and just AATSR respectively detect ash. The higher occurrence of blue points than green ones shows that there are more grid boxes where ash is being detected by AATSR than by IASI, hence suggesting that IASI is slightly less sensitive to ash (i.e., has a slightly higher detection threshold concentration).

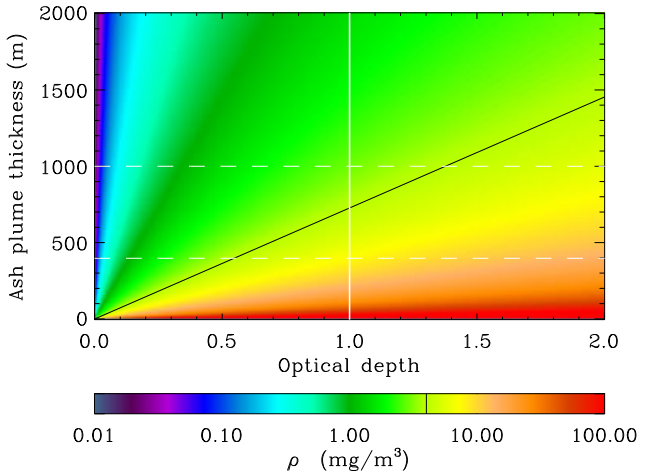

Figure 3. The concentrations of ash present at different optical depths for different thicknesses of plume (assumed homogeneous). The white vertical line denotes the detection threshold for the AATSR satellite, the horizontal dashed lines denote the probable range of geometrical plume thicknesses given by *Winker et al.* [2012], and the black line corresponds to a concentration of $4\,mg\,m^{-3}$.

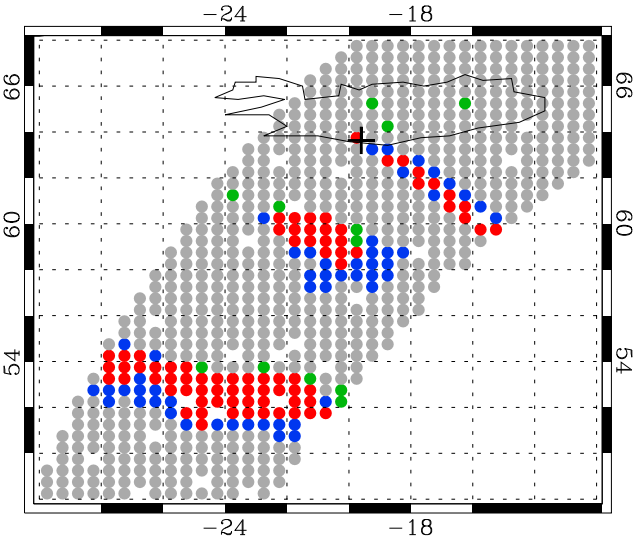

Figure 4. Results from 9 May 2010 for comparison between the ash detection of IASI and AATSR. (grey) Neither satellite detects ash; (green) Only IASI detects ash; (blue) Only AATSR detects ash; (red) Both satellites detect ash.

3. Studies of Particular Eruptions

3.1. Eyjafjallajökull 2010

[30] In April and May 2010, there was a major eruption of the Eyjafjallajökull volcano, Iceland (63.63°N, 19.62°W; 1666 m a.s.l.), with the main explosive phase of the eruption beginning on 14 April. IASI data from the period 14 April to 17 May were studied, with two images per day. A more limited sampling of AATSR images (due to its narrow swath) were also available for comparison with IASI, so the behavior of the two species could be observed over the period of a whole month.

[31] Four days were looked at in detail, and results from the entire period analyzed. Figure 5 shows the maps for the 4 days of interest using ash and SO_2 flags from IASI, while Figure 6 shows the corresponding images using AATSR for the ash detection. The missed ash fraction, as defined in section 2, can be thought of as the number of blue points in these figures, divided by the number of blue plus red points.

[32] The IASI calculations used a grid box of side length equivalent to 0.1° longitude and latitude, while those using the AATSR ash flag used a grid box of side length equivalent to 0.5° longitude and latitude. The region covered in the IASI case was 50°W–40°E, 45°N–70°N, while due to its smaller swath width, the AATSR region was smaller and covered 30°W–10°E, 48°N–72°N. The IASI ash flag used a threshold value of six retrievals flagging high optical depth (out of a total of 24) to indicate the presence of ash, while the AATSR flag used the thresholds defined in equations (7) and (8).

[33] The initial stages of the eruption were characterized by strong ash emission, but little SO_2 [*Thomas and Prata*, 2011]. This is probably partly due to the fact that the eruption occurred from beneath a glacier, and so initially, there was a lot of ice and water present, meaning much of the SO_2 could react via equations (1)–(3) to form sulphuric acid before making it into the distal ash cloud observed from space. This can be seen in Figure 5a which shows the area on 15 April. The red points denote collocation of ash and SO_2 and show that the two species are strongly correlated for much of the plume. However a certain amount of separation of species is

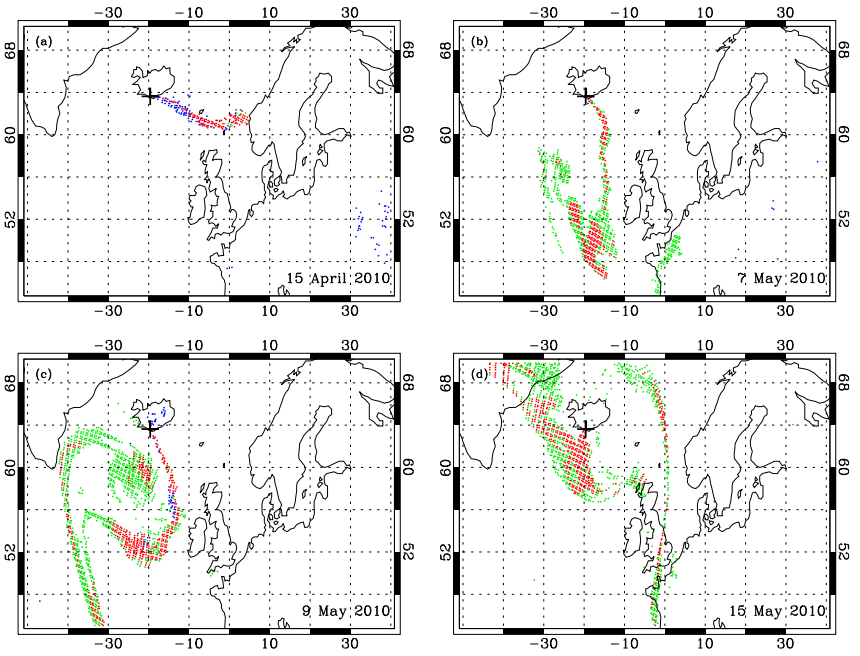

Figure 5. The location of ash and SO_2 from the Eyjafjallajökull eruption for the mornings of (a) 15 April, (b) 7 May, (c) 9 May, and (d) 15 May 2010 using the IASI SO_2 and ash flags. In each map the black cross marks the location of the volcano. (red) Both ash and SO_2 are present; (blue) Only SO_2 is present (green); Only ash is present.

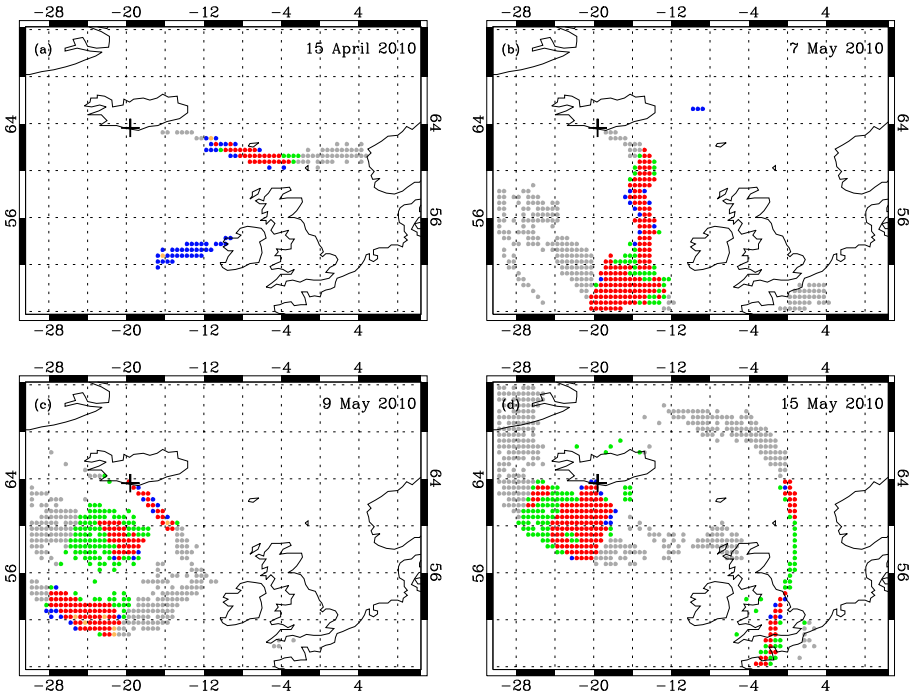

Figure 6. The location of ash and SO_2 from the Eyjafjallajökull eruption for the mornings of (a) 15 April, (b) 7 May, (c) 9 May, and (d) 15 May 2010 using the IASI SO_2 and AATSR ash flags. In each map the black cross marks the location of the volcano. (red) Both ash and SO_2 are present; (green) Only SO_2 is present; (blue) Only ash is present; (grey) No AATSR data, but SO_2 is present; (orange) No IASI data, but ash is present.

evident, with the blue and green points representing just ash and just SO_2, respectively. This agrees with what Thomas and Prata found in their study using data from the Spinning Enhanced Visible and Infrared Imager (SEVIRI) and Ozone Monitoring Instrument (OMI) [*Thomas and Prata*, 2011]. Figure 6a shows the corresponding plot using AATSR for ash detection, which appears to agree very closely with that from IASI in the plume. One major anomaly is the apparent additional ash cloud off the west coast of Ireland. However, when this is studied using a false color image of the AATSR data, this cloud is not visible and does not show up noticeably on visual inspection of a plot of the brightness temperature difference described in section 1.2.2. Therefore, it must be concluded that this is a false positive result, possibly due to ice cloud, which can affect AATSR retrieval. Further suspected false positives are evident in the IASI image in a region around 52°N, 35°E. The reason for these is unknown.

[34] Following this initial explosive phase, there followed a much quieter period with very little long range ash transport. The lull in activity was observed in the results from IASI and AATSR with only relatively few points flagging ash or SO_2 during this period. This was followed by a further period with stronger ash and gas emission from 5 May [*Prata and Prata*, 2012]. The increase in activity was also observed by IASI and AATSR. The next date shown is 7 May (Figures 5b and 6b). The IASI plot shows some significant areas of collocation throughout the plume, but also a significant quantity of SO_2 without corresponding ash. From an aviation safety situation, this appears to be a scenario where, if SO_2 were used as a proxy, it would overestimate the region containing ash. The corresponding AATSR image also gives the same result for the region covered by the AATSR swath, as does the information presented by *Thomas and Prata* [2011]. Their data also highlight the fact that, in general, it is regions of low SO_2 concentration which lack corresponding ash detection. Thus, there is the possibility that ash is in fact present here, but in concentrations below the detection threshold of the instruments. As discussed in section 2.2, it is possible that this ash is still in concentrations that exceed the high contamination threshold.

[35] Figures 5c and 6c show the situation on 9 May. The IASI plot (Figure 5c) clearly shows the long SO_2 plume and suggests that ash collocation only occurs in certain areas of the plume. The AATSR plot (Figure 6c) backs up this suggestion, although the fact that AATSR only covers a narrow region of the map means that it cannot be used to verify all of the IASI information. Once again, in both figures, there is the possibility that areas which are detected as containing only SO_2 may in fact contain ash at concentrations below the detection thresholds for the two satellites, but potentially above the high contamination threshold. Figure 7 shows an indication of the column amount of SO_2 present in each pixel for IASI, as retrieved using the method of *Carboni et al.* [2012], and Figure 8 shows the brightness temperature difference (described in section 1.2.2) for the AATSR data, which gives a first-order indication of the amount of ash present. The feature which is easy to identify in all the plots for this particular day is the region of collocation centered at around 59°N, 20°W, which is visible as a "pool" of red points in Figures 5c and 6c. It can be seen from Figure 7 that this region is where the SO_2 concentration

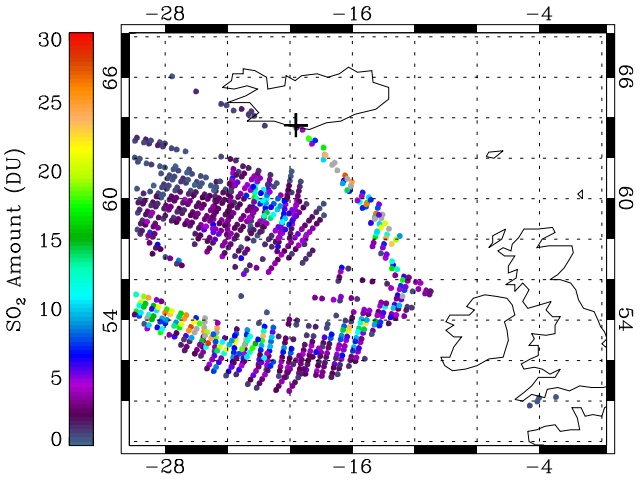

Figure 7. Amount of SO_2 from the Eyjafjallajökull eruption for the morning of 9 May 2010. The black cross marks the location of the volcano.

is highest in this part of the cloud (with a column amount of ∼10 DU), while the surrounding concentrations are low (<5 DU). From the ash map (Figure 8), it is clear that even where ash is detected in the area around 59°N, 20°W, the amount present is significantly less than in the main plume as evidenced by brightness temperature differences approaching zero. Hence, the ash may well be present in the whole cloud, but undetectable.

[36] The final images to be studied are those from 15 May (Figures 5d and 6d). The IASI image again clearly shows a large plume of gases, with ash only showing up for a certain proportion of the plume. As for the other dates, this is essentially mirrored by the AATSR map, but with the AATSR map perhaps showing slightly more ash, further suggesting the possibility of a slightly lower detection threshold as found earlier. What should be noted is the lack of blue points in all of the panels shown from this later part of the eruption, demonstrating that although SO_2 frequently appears without any corresponding ash, the converse is rarely true, which may suggest that SO_2 could serve as a conservative proxy for the possible presence of ash. However, this will be examined in more detail below and shown not always to be the case.

3.2. Puyehue 2011

[37] Beginning in June 2011, there was a volcanic eruption from the Puyehue-Cordón Caulle volcanic complex, Chile (40.5°S, 72.2°W; 1793 m a.s.l.). IASI covered the whole region twice a day and data from 5 June to 2 July were studied. One AATSR snapshot was available for each day from 6 to 9 June. However the limited coverage of AATSR meant that these images were of very limited benefit and so were only used for the verification of the IASI ash flag around the crater (see below). The distal ash cloud from this eruption eventually circled the globe and caused the cancelation of flights from Australia and New Zealand (http://earthobservatory.nasa.gov/NaturalHazards/view.php?id=50985). For this case the region used for study was 180°W–180°E (i.e., the entire longitude range), and 58°S–24°S. For the majority of the region, the same IASI ash flag threshold was used as for the Eyjafjallajökull eruption to minimize noise, while maximizing the ash detection. However, the high concentrations of ash around the volcano and the high altitude of the plume meant that the ash flag failed to work correctly and missed significant areas where ash had been detected and confirmed by AATSR. Because of this, for a small region around the crater itself, a lower ash flag threshold value was used in order to pick up ash in this region.

[38] One example plot from this eruption (9 June 2011) is given in Figure 9. Close to the volcano, there is an area with a significant amount of ash present without any corresponding SO_2 (although this could be partly due to the forced lower flag threshold mentioned above). There is also a large volcanic cloud stretching across the ocean toward Australia and New Zealand. This cloud, as for most of those seen for Eyjafjallajökull, shows collocation for a lot of its area, with the remainder being flagged as containing SO_2 but no ash. Again, it may be that undetectable, but potentially exceeding the high contamination threshold, ash is present even in the regions where it is not being flagged.

4. Analysis

[39] The missed ash fraction calculation described in section 2 was applied to the gridded data, as shown in Figures. 5, 6 and 9, for the full period of each eruption and plotted as a function of time since the start of the eruption (bottom panels in Figures 10 and 11). The top panels in each case show the total number of grid boxes, which were flagged as containing ash on each day. The day to day variability of the plotted quantity is indicated by the error bars, which are the RMS of the difference between the plotted value on successive days. These plots do not relate simply to the evolution of the ash cloud with time or distance traveled from the volcano, since they show the results for the entire ash and SO_2 clouds, regardless of emission time. However, they do serve to show the level of consistency in the correspondence of the two products. It can immediately be seen that the amount of ash missed shows considerable variability over time.

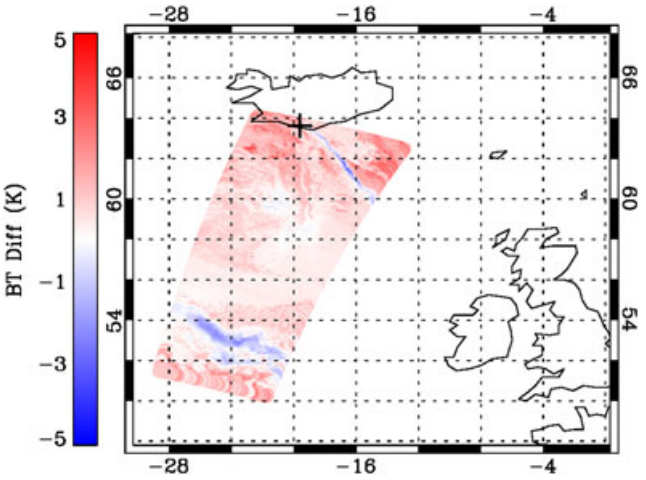

Figure 8. Brightness temperature difference between the 10.8 μm and 12 μm channels of AATSR for the Eyjafjallajökull eruption for the morning of 9 May 2010. The black cross marks the location of the volcano.

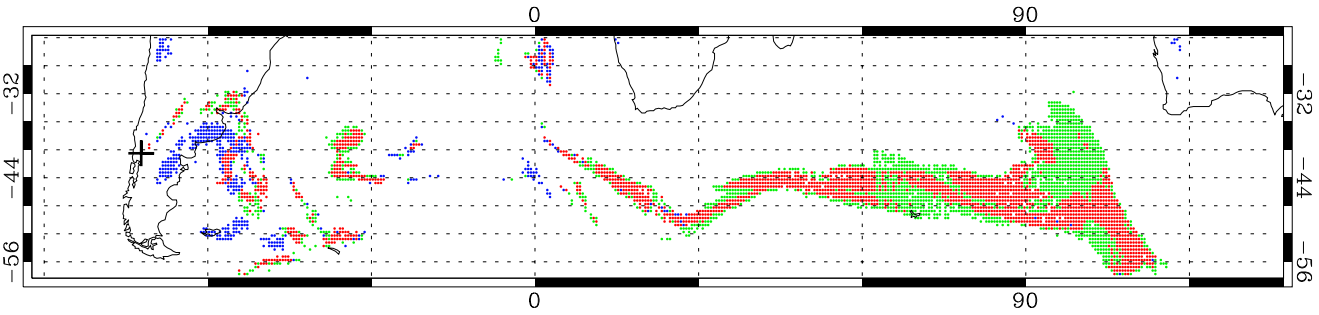

Figure 9. The location of ash and SO_2 from the Puyehue eruption for the morning of 9 June 2011 using the IASI SO_2 and ash flags. The black cross marks the location of the volcano. (red) Both ash and SO_2 are present; (green) Only SO_2 is present; (blue) Only ash is present.

[40] For Eyjafjallajökull, the missed ash fraction was calculated using both the IASI and the AATSR ash flags. The results from the two satellites appear to agree reasonably well, despite the fact that the AATSR data set is from a much smaller geographical region, and in nearly all cases, the AATSR data point lies within the error bar of the corresponding IASI point. As mentioned before, there was a period of low activity, which is clearly observed by the low number of points containing ash from 21 April to 4 May (7–20 days from the start of the eruption). The reasonably large missed ash fractions evident during the active periods, particularly before this lull in the eruption, are cause for concern. The general trend for the data from Eyjafjallajökull, ignoring the lull period, seems to be that the success of using SO_2 as a proxy increases toward the end of the eruption, with a >90% agreement over the last week of the eruption. However, over the first few days of the eruption, using SO_2 as a proxy would miss over 50% of the ash, pointing to the necessity of direct ash detection.

[41] These results can be compared to the analysis carried out by *Thomas and Prata* [2011]. This work examined a range of SO_2 products (as listed in the previous section) and included comparisons to the Met Office NAME model and extinction profiles from the CALIOP spaceborne lidar, in addition to the SEVIRI ash flag, and came to broadly similar conclusions that although the ash and SO_2 clouds were often collocated, they could not be used as proxies for each other. However, the range of different spatiotemporal sampling of the data sets used prevented a direct point by point comparison.

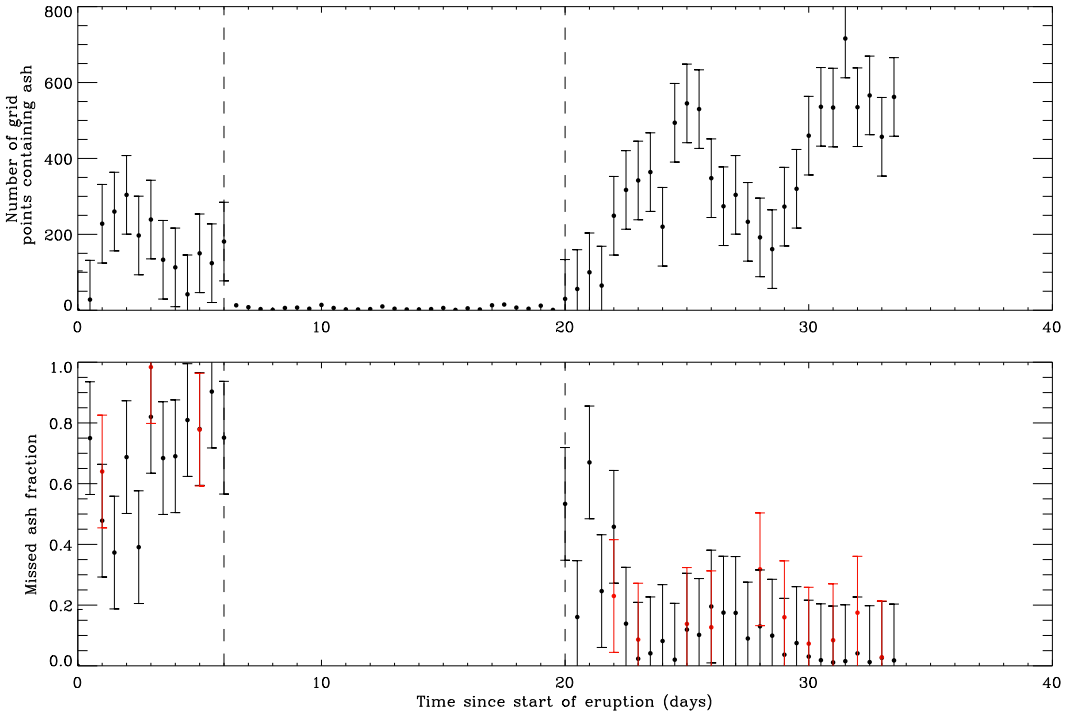

Figure 10. (top) The number of grid boxes where ash was detected as a function of time for the Eyjafjallajökull eruption. (bottom) The missed ash fraction as a function of time for the Eyjafjallajökull eruption. The black points show the data using the IASI ash flag, while the red points show the data using the AATSR ash flag. The region between the vertical dashed lines indicates a period of low emissions, and so the missed ash fraction is not included for this period.

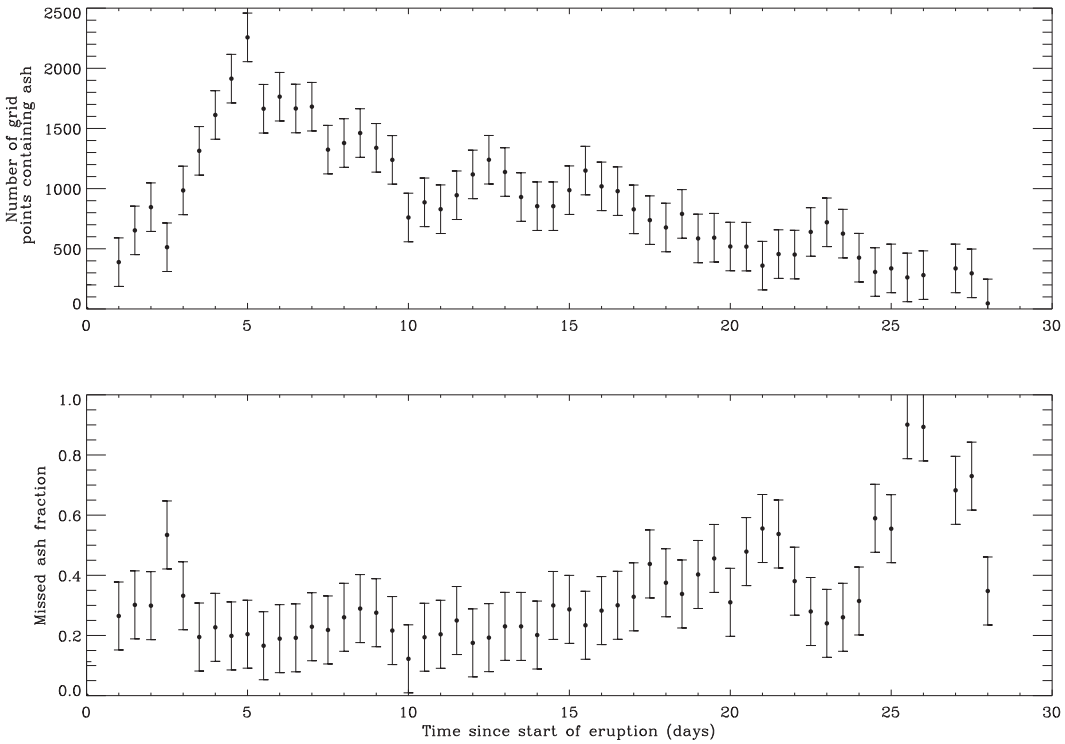

Figure 11. (top) The number of grid boxes where ash was detected as a function of time for the Puyehue eruption using the IASI ash flag. (bottom) The missed ash fraction as a function of time for the Puyehue eruption using the IASI ash flag.

[42] For the eruption of Puyehue, the mean amount of ash missed is 33%. Furthermore, there is no dramatic lull in the eruption here, as evidenced in Figure 11 (top), where the number of ash points remains relatively high throughout. In most of the maps for this eruption, it is evident that the vast majority of the points where ash is flagged without corresponding SO_2 are close to the volcano itself. This is perhaps counterintuitive, but it could well be that there is in fact SO_2 present here, which is not being picked up due to the large amounts of ash masking the SO_2 detection. Nevertheless, if the SO_2 is not detectable, then it is no good as a proxy for ash, whether it is actually present or not. In an opposite trend to the case of Eyjafjallajökull, the missed ash fraction shows an upward trend, rising from $\sim$20% during the first half of the eruption to frequent values of over 50% in the last 10 days. This is believed to be due to the wind conditions during this particular case study, which may have caused the species to separate more in the later part of the eruption. Also, for Puyehue, the cloud extended around an entire latitude circle over the course of approximately 1 week, providing more opportunity for the ash and SO_2 to separate and for SO_2 to be oxidized.

[43] The data from the Puyehue eruption further show that SO_2 is not a suitable proxy to use, since missing $\sim$ 30% of ash is definitely not acceptable. The differing trends between the eruptions studied demonstrates that there is no clear and predictable pattern which can be adopted, and eruptions must be studied on a case-by-case basis.

[44] The missed ash fractions only provide a very rough indication of how much ash is being missed in each case and give a spatial fraction rather than a fraction by mass, as any amount of detectable ash or SO_2 within each grid box causes the box to be flagged as containing that species, regardless of concentration. The flags themselves have some potential problems (as discussed in section 1.2), causing ash or SO_2 to remain undetected when they are in fact present, and also causing false positive detections due to water or ice cloud, or just due to inherent noise in the retrievals. On top of these, the methods involved have introduced some further uncertainty; first, not all the ash or SO_2 from the eruption is necessarily included in the calculations, as the calculations are only taken over a certain geographical region, so any ash or gases outside this particular zone will not be included. Furthermore, the resolution for Eyjafjallajökull is only 0.1° longitude and latitude at best, and for Puyehue, it is only 0.5° longitude and latitude, which can cause some errors, particularly at the edges of the plumes. The errors have been estimated from the obtained data by taking the RMS value of the differences between each successive measurement of missed ash fraction and total ash fraction for the IASI data. Since consecutive points from AATSR are not necessarily on consecutive days, the error on these measurements cannot be estimated directly, and so have been assumed to be equal to the errors found in the IASI case. In reality, the errors for AATSR may be slightly higher due to the coarser grid used in the analysis of the data.

[45] Some ash exceeding the high contamination threshold will remain undetected by IASI and AATSR, which will cause a slight departure in each calculation from the "true" missed ash fraction. Whether it has overestimated or underestimated the amount of missed ash cannot be specified, as it depends on the location of the undetected ash. An educated

guess would lead us to suspect that the undetected ash is located on the green points on the plots (i.e., in the locations flagged as containing SO_2 but no ash) immediately adjacent to points where ash is detected (i.e., red points), which would thus improve (lower) the missed ash fraction if all ash was detected. Where strong vertical wind shear has affected the volcanic cloud, this may not be the case and ash may in fact exist at locations without any SO_2. For different eruptions, which may have slightly different ash properties, the exact flag thresholds will vary slightly, so it can never be assumed that all ash is being detected.

5. Conclusions

[46] Comparisons of volcanic SO_2 detected by the IASI instrument and volcanic ash detected by the IASI and AATSR instruments from the 2010 eruption of Eyjafjallajökull and the 2011 eruption of Puyehue-Cordón Caulle have been compared, using the concept of a missed ash fraction based on regridded data. For both eruptions the emitted SO_2 and ash clouds showed considerable coincidence on visual inspection. The calculated missed ash fractions showed that in some instances using SO_2 as a proxy for the location of the ash cloud would result in less than 10% of the satellite detected ash being missed, although the overall area of ash contamination would be substantially over estimated, particularly during the later stages of the Eyjafjallajökull eruption. However, the degree collocation was found to be very variable, both between the two eruptions and throughout the course of each eruption. On the worst days, more than 80% of the observed ash cloud was found to be not coincident with detected SO_2.

[47] Reasons for this variability include the separation of the clouds due to wind shear and differences in the atmospheric life times of the two species [*Thomas and Prata*, 2011; *Prata and Kerkmann*, 2007]. Limitations of the two detection schemes, such as masking of ash by ice or water clouds, or the masking of SO_2 spectral signatures by very high ash loading, also contribute.

[48] It is clear that satellite sensors can provide valuable detection of both ash and SO_2, at sensitivities that are of relevance to aircraft safety, but neither method is 100% reliable and one can certainly not be taken as a proxy for the other. Given the wide range of both UV and infrared instruments which are capable of detecting SO_2, as well as the limitations of ash detection from space, the use of satellite SO_2 products in mitigating the aviation hazard is clearly justified, both in detecting the occurrence of eruptions in remote locations and as an initial indicator of areas that present a potential aviation hazard. However, direct ash detection by satellite is also required.

[49] The simplicity and speed of simple ash and SO_2 detection algorithms, such as those used here, makes them suitable for adaptation to operational near-real-time products, which should greatly improve confidence in the dispersion models used by the VAACs.

[50] **Acknowledgments.** The authors would like to thank Patrick Watts, Adam Povey, and Daniel Peters for their input to this paper. This work was partly funded by the UK Natural Environment Research Council (NERC) National Centre for Earth Observation (NCEO) and the NERC VANAHEIM project NE/1015592/1.

References

Bernard, A., and W. Rose (1990), The injection of sulfuric acid aerosols in the stratosphere by the El Chichón volcano and its related hazards to the international air traffic, *Nat. Hazards*, *3*, 59–67, doi:10.1007/BF00144974.

Bogumil, K., et al. (2003), Measurements of molecular absorption spectra with the SCIAMACHY pre-flight model: Instrument characterization and reference data for atmospheric remote-sensing in the 230–2380 nm region, *J. Photoch. Photobio. A*, *157*(2-3), 167–184, doi:10.1016/S1010-6030(03)00062-5.

Carboni, E., R. Grainger, J. Walker, A. Dudhia, and R. Siddans (2012), A new scheme for sulphur dioxide retrieval from IASI measurements: Application to the Eyjafjallajökull eruption of April and May 2010, *Atmos. Chem. Phys.*, *12*(23), 11417–11434, doi:10.5194/acp-12-11417-2012.

Carn, S., A. Krueger, N. Krotkov, K. Yang, and K. Evans (2009), Tracking volcanic sulfur dioxide clouds for aviation hazard mitigation, *Nat. Hazards*, *51*, 325–343, doi:10.1007/s11069-008-9228-4.

Casadevall, T. J. (1994), The 1989–1990 eruption of Redoubt volcano, Alaska: Impacts on aircraft operations, *J. Volcanol. Geoth. Res.*, *62*(1–4), 301–316.

Casadevall, T. J., and T. M. Murray (2000), Advances in volcanic ash avoidance and recovery, *Boeing Aero Mag.*, *9*, 19–27, http://www.boeing.com/commercial/aeromagazine/aero_09/volcanic_story.html, Accessed 25 July 2012.

Civil Aviation Authority, (2011), Guidance regarding flight operations in the vicinity of volcanic ash, *CAA Technical Notice, SN-2011/004*, http://www.caa.co.uk/docs/1425/20110526GuidanceRegardingFlightOperationsInTheVicinityOfVolcanicAsh.pdf, Accessed 27 July 2012.

Clarisse, L., P. F. Coheur, A. J. Prata, D. Hurtmans, A. Razavi, T. Phulpin, J. Hadji-Lazaro, and C. Clerbaux (2008), Tracking and quantifying volcanic SO_2 with IASI, the September 2007 eruption at Jebel at Tair, *Atmos. Chem. Phys.*, *8*(24), 7723–7734, doi:10.5194/acp-8-7723-2008.

Clarisse, L., F. Prata, J.-L. Lacour, D. Hurtmans, C. Clerbaux, and P. F. Coheur (2010), A correlation method for volcanic ash detection using hyperspectral infrared measurements, *Geophys. Res. Lett.*, *37*, L19806, doi:10.1029/2010GL044828.

Clarisse, L., P.-F. Coheur, F. Prata, J. Hadji-Lazaro, D. Hurtmans, and C. Clerbaux (2012), A unified approach to infrared aerosol remote sensing and type specification, *Atmos. Chem. Phys.*, *13*(4), 2195–2221, doi:10.5194/acp-13-2195-2013.

Clerbaux, C., et al. (2009), Monitoring of atmospheric composition using the thermal infrared IASI/Metop sounder, *Atmos. Chem. Phys.*, *9*(16), 6041–6054, doi:10.5194/acp-9-6041-2009.

Derimian, Y., O. Dubovik, D. Tanre, P. Goloub, T. Lapyonok, and A. Mortier (2012), Optical properties and radiative forcing of the Eyjafjallajökull volcanic ash layer observed over Lille, France, in 2010, *J. Geophys. Res.*, *117*, D00U25, doi:10.1029/2011JD016815.

Francis, P. N., M. C. Cooke, and R. W. Saunders (2012), Retrieval of physical properties of volcanic ash using Meteosat: A case study from the 2010 Eyjafjallajökull eruption, *J. Geophys. Res.*, *117*, D00U09, doi:10.1029/2011JD016788.

Grainger, R. G., D. M. Peters, G. E. Thomas, A. Smith, R. Siddans, E. Carboni, and A. Dudhia (2013), Measuring volcanic plume and ash properties from space, in remote sensing of volcanoes and volcanic processes: Integrating observation and modelling, *Geol. Soc. Spec. Publ.*, *380*, doi:10.1144/SP380.7, in press.

ICAO (2007), *Manual on Volcanic Ash, Radioactive Material, and Toxic Chemical Clouds* (2nd edn), International Civil Aviation Organization, Doc. 9691, AN/954, Montreal, Canada. http://www.paris.icao.int/news/pdf/9691.pdf, Accessed 11 July 2012.

International Federation of Airline Pilots' Associations (2011), *Flight operations in the presence of volcanic contamination*. Aircraft Design & Operation Committee Statement, *12POS01*, http://www.ifalpa.org/ifalpa-statements/aircraft-design-a-operation.html, Accessed 11 July 2012.

Institution of Mechanical Engineers, (2010), Volcanic ash: To fly or not to fly, *Tech. Rep.*, Institution of Mechanical Engineers.

Johnson, B., et al. (2012), In situ observations of volcanic ash clouds from the FAAM aircraft during the eruption of Eyjafjallajökull in 2010, *J. Geophys. Res.*, *117*, D00U24, doi:10.1029/2011JD016760.

Llewellyn Jones, D. (1993), Precise sea-surface temperature measurement from the ERS-1 satellite—A Climate Challenge, *Endeavour*, *17*(2), 52–59, doi:10.1016/0160-9327(93)90197-B.

Marenco, F., B. Johnson, K. Turnbull, S. Newman, J. Haywood, H. Webster, and H. Ricketts (2011), Airborne lidar observations of the 2010 Eyjafjallajökull volcanic ash plume, *J. Geophys. Res.*, *116*, D00U05, doi:10.1029/2011JD016396.

Niemeier, U., C. Timmreck, H.-F. Graf, S. Kinne, S. Rast, and S. Self (2009), Initial fate of fine ash and sulfur from large volcanic eruptions, *Atmos. Chem. Phys.*, *9*(22), 9043–9057, doi:10.5194/acp-9-9043-2009.

Pergola, N., V. Tramutoli, F. Marchese, I. Scaffidi, and T. Lacava (2004), Improving volcanic ash cloud detection by a robust satellite technique, *Remote Sens. Environ.*, *90*(1), 1–22, doi:10.1016/j.rse.2003.11.014.

Prata, A. (1989), Observations of volcanic ash clouds in the 10–12 μm window using AVHRR/2 data, *Int. J. Remote Sens.*, *10*(4-5), 751–761.

Prata, A. J., and J. Kerkmann (2007), Simultaneous retrieval of volcanic ash and SO_2 using MSG-SEVIRI measurements, *Geophys. Res. Lett.*, *34*, L05813, doi:10.1029/2011JD016800.

Prata, A. J., and A. T. Prata (2012), Eyjafjallajökull volcanic ash concentrations determined using Spin Enhanced Visible and Infrared Imager measurements, *J. Geophys. Res.*, *117*, D00U23, doi:10.1029/2006GL028691.

Przedpelski, Z. J., and J. Casadevall (1994), Impact of volcanic ash from 15 December 1989 Redoubt volcanic eruption on GE CF6-80C2 turbofan engines, in *Volcanic Ash and Aviation Safety: Proceedings of the First International Symposium on Volcanic Ash and Aviation Safety,* July 1991, pp. 129–135, U.S. Geological Survey Bulletin 2047, Seattle, Washington.

Robock, A. (2000), Volcanic eruptions and climate, *Rev. Geophys.*, *38*(2), 191–219.

Rodgers, C. D. (2000), *Inverse Methods for Atmospheric Sounding: Theory and Practice*, pp. 65–72, World Scientific Publishing Co., Singapore.

Rose, W. I., G. J. S. Bluth, and G. G. J. Ernst (2000), Integrating retrievals of volcanic cloud characteristics from satellite remote sensors: A summary, *Phil. Trans. R. Soc. A.*, *358*(1770), 1585–1606, doi:10.1098/rsta.2000.0605.

Schneider, D., W. Rose, L. Coke, G. Bluth, I. Sprod, and A. Krueger (1999), Early evolution of a stratospheric volcanic eruption cloud as observed with TOMS and AVHRR, *J. Geophys. Res.*, *104*(D4), 4037–4050, doi:10.1029/1998JD200073.

Smith, D., J. Delderfield, D. Drummond, T. Edwards, C. Mutlow, P. Read, and G. Toplis (2001), Calibration of the AATSR instrument, *Adv. Space Res.*, *28*(1), 31–39, doi:10.1016/S0273-1177(01)00273-3.

Stamnes, K., S.-C. Tsay, W. Wiscombe, and K. Jayaweera (1988), Numerically stable algorithm for discrete-ordinate-method radiative transfer in multiple scattering and emitting layered media, *Appl. Optics*, *27*(12), 2502–2509, doi:10.1364/AO.27.002502.

Stohl, A., et al. (2011), Determination of time- and height-resolved volcanic ash emissions and their use for quantitative ash dispersion modeling: The 2010 Eyjafjallajökull eruption, *Atmos. Chem. Phys.*, *11*(9), 4333–4351, doi:10.5194/acp-11-4333-2011.

Thomas, H. E., and A. J. Prata (2011), Sulphur dioxide as a volcanic ash proxy during the April–May 2010 eruption of Eyjafjallajökull Volcano, Iceland, *Atmos. Chem. Phys.*, *11*(14), 6871–6880, doi:10.5194/acp-11-6871-2011.

Turnbull, K., B. Johnson, F. Marenco, J. Haywood, A. Minikin, B. Weinzierl, H. Schlager, U. Schumann, S. Leadbetter, and A. Woolley (2012), A case study of observations of volcanic ash from the Eyjafjallajökull eruption: 1. In situ airborne observations, *J. Geophys. Res.*, *117*, D00U12, doi:10.1029/2011JD016688.

van der A, R., et al. (2010), *GMES service element Promote 2, S3 service prospectus, Ver. 3, report*, pp. 54, European Space Agency, Paris.

Vogel, L., et al. (2011), Early in-flight detection of SO_2 via differential optical absorption spectroscopy: A feasible aviation safety measure to prevent potential encounters with volcanic plumes, *Atmos. Meas. Tech.*, *4*(9), 1785–1804, doi:10.5194/amt-4-1785-2011.

Walker, J. C., A. Dudhia, and E. Carboni (2011), An effective method for the detection of trace species demonstrated using the MetOp Infrared Atmospheric Sounding Interferometer, *Atmos. Meas. Tech.*, *4*(8), 1567–1580, doi:10.5194/amt-4-1567-2011.

Walker, J. C., E. Carboni, A. Dudhia, and R. G. Grainger (2012), Improved detection of sulphur dioxide in volcanic plumes using satellite-based hyperspectral infrared measurements: Application to the Eyjafjallajökull 2010 eruption, *J. Geophys. Res.*, *117*, D00U16, doi:10.1029/2011JD016810.

Ward, P. L. (2009), Sulfur dioxide initiates global climate change in four ways, *Thin Solid Films*, *517*(11), 3188–3203, doi:10.1016/j.tsf.2009.01.005.

Webster, H. N., et al. (2012), Operational prediction of ash concentrations in the distal volcanic loud from the 2010 Eyjafjallajökull eruption, *J. Geophys. Res.*, *117*, D00U08, doi:10.1029/2011JD016790.

Wen, S., and W. I. Rose (1994), Retrieval of sizes and total masses of particles in volcanic clouds using AVHRR bands 4 and 5, *J. Geophys. Res.*, *99*(D3), 5421–5431, doi:10.1029/93JD03340.

Winker, D. M., Z. Liu, A. Omar, J. Tackett, and D. Fairlie (2012), CALIOP observations of the transport of ash from the Eyjafjallajökull volcano in April 2010, *J. Geophys. Res.*, *117*, D00U15, doi:10.1029/2011JD016499.

Zehner, C. (ed.) (2012), *Monitoring Volcanic Ash from Space—ESA-EUMETSAT Workshop on the 14 April to 23 May 2010 Eruption at the Eyjafjöll volcano, South Iceland*, ESA-ESRIN, 26–27 May 2010, ESA-Publication STM-280, Frascati, Italy, doi:10.5270/atmch-10-01.